Journal of Nuclear Materials 385 (2009) 358–363

Contents lists available at ScienceDirect

Journal of Nuclear Materials

journal homepage: www.elsevier.com/locate/jnucmat

# Computer simulations of non-congruent melting of hyperstoichiometric uranium dioxide

M.J. Welland [a], W.T. Thompson [a], B.J. Lewis [a,*], D. Manara [b]

[a] Department of Chemistry and Chemical Engineering, Royal Military College of Canada, P.O. Box 17000, Station Forces, Kingston, Ontario, Canada K7K 7B4
[b] European Commission, Joint Research Centre, Institute for Transuranium Elements, P.O. Box 2340, 76125 Karlsruhe, Germany

A B S T R A C T

Detailed models of $UO_{2+x}$ at very high temperatures incorporating the effects of non-congruent melting have been developed to support the design and analysis of experimental work related to nuclear safety. Models based on both the Stefan formulation and phase field approach are implemented using recently published material properties. Simulations compare well with laser flash experiments performed on $UO_{2+x}$. This work has application in modelling centreline melting of defective fuel which may occur due to the reduced thermal conductivity and lower incipient melting temperature associated with fuel oxidation.



## 1. Introduction

In the event of upset or very high power conditions, it is possible that the temperature at the centreline of a fuel pellet will exceed the local melting point and begin to melt. This possibility is enhanced if the fuel element has become defective, in which case the coolant is allowed to contact the $UO_2$, oxidizing it to $UO_{2+x}$. Hyperstoichiometric fuel has a reduced thermal conductivity and a lower incipient melting point, thus reducing the margin of safety preventing the formation of molten fuel.

The thermal and mechanical implications of molten fuel under upset or severe reactor accident conditions have been previously modelled on a large scale for the purpose of reactor safety [1–5]. Detailed simulations have been conducted for defective fuel elements under normal operating conditions [6–8], however, these simulations do not cover the possibility of a molten phase. Thus a treatment is need for these conditions.

Laser flash experiments have been performed recently at the Institute for Transuranium Elements in order to better understand the thermal properties of $UO_2$ at high temperatures in both the solid and liquid states. In particular, the precise placement of the solidus and liquidus lines are of interest in order to predict the onset of centreline melting [9,10]. In order to determine such properties, sophisticated models coupling the heat and mass transport are typically needed [11].

This work therefore details the parallel development of two modelling techniques, the Stefan formulation and the Phase Field model, towards the analysis of experimentation involving non-congruent phase change and to later be developed to simulate fuel centreline melting in operational nuclear fuel. The parallel development of two types of models allows for a check of consistency between the different techniques, which encourages confidence in the simulation implementation and focuses attention on the material properties at very high temperatures and the phase diagram. This model builds on the stoichiometric model presented in [12].

## 2. Modelling technique

Through experiments in self-diffusion, it was discovered that the mobility of oxygen atoms is much larger than that of uranium [13]. Therefore, $UO_{2+x}$ is modelled as an immobile $UO_2$ lattice with a mobile species of interstitial oxygen atoms, the ratio of the later to the former being represented by $x$. The inclusion of the thermodynamic functions involves the integration of the thermodynamics and kinetics of the system on a fundamental level.

Local equilibrium is assumed at the interface at all times in accordance with the phase diagram in Fig. 1. Modifications to this phase diagram have been proposed [9,14], however, the thermodynamic model presented in [6], which produces the phase diagram in Fig. 1, is retained at this point for the purpose of consistency with previous work.

Both the Stefan and the Phase Field model rely on the formulation of the heat and mass fluxes. Derivation of these fluxes is accomplished through the Theory of Irreversible Processes (Non-equilibrium Thermodynamics) [15] which provides the fundamental interrelation of the evolution of the thermodynamic state variables with the thermodynamics of the system including the Soret effect [16], the Dufour effect [17], the chemical diffusion coefficient, and phase stability.

* Corresponding author. Tel.: +1 613 541 6000x6611; fax: +1 613 542 9489.
E-mail address: lewis-b@rmc.ca (B.J. Lewis).

0022-3115/$ - see front matter Crown Copyright © 2008 Published by Elsevier B.V. All rights reserved.
doi:10.1016/j.jnucmat.2008.12.023

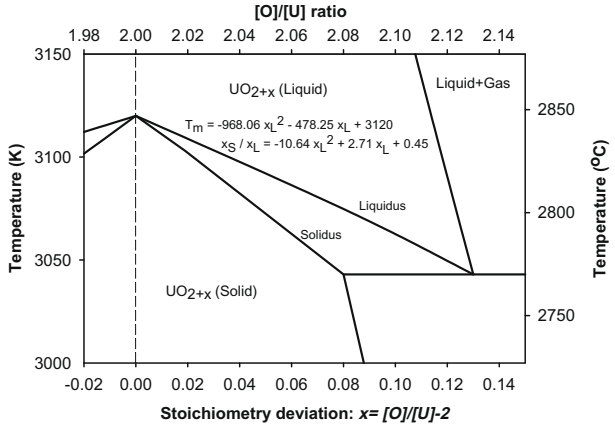


**Fig. 1.** Computed U–O binary phase diagram at 1 atm from reference [6], showing fit temperature and partition coefficient functions used as inputs to the model.

Due to the small thermal expansion of condensed phases, the volume is assumed to be constant as an approximation. Therefore, in order to conserve mass, the density is treated as a constant. The approximation of constant volume also implies that the thermodynamic functions of internal energy and enthalpy (and therefore the Helmholtz and Gibbs energy) are equal.

### 2.1. Mass and heat fluxes

The transport of heat and mass is able to be derived through the Theory of Irreversible Processes as described in Appendix A. Through this formulation, it is concluded that in order for the entropy of a system to increase as a result of irreversible processes, the heat and mass flux must obey the following inequality:

$$-\frac{1}{T^2}\nabla T\cdot\vec{q}-\frac{1}{T}\nabla\mu_T\cdot\vec{J}_o\geqslant 0, \tag{1}$$

where $T$ is the temperature, $q$ is the conductive heat flux, $\mu$ is the chemical potential of interstitial oxygen and $J_o$ is the flux of interstitial oxygen. The subscript $T$ beside $\mu$ indicates that the gradient is taken at constant temperature. This inequality may be assured by introducing linear phenomenological laws relating all thermodynamic state variables to the thermodynamic driving forces:

$$\begin{bmatrix}\vec{q}\\ \vec{J}_o\end{bmatrix}=\begin{bmatrix}M_{qq} & M_{qo}\\ M_{oq} & M_{oo}\end{bmatrix}\begin{bmatrix}-\nabla T/T^2\\ -\nabla\mu_T/T\end{bmatrix}, \tag{2}$$

where the matrix is positive definite. The elements of this matrix are the 'mobilities' which describe a linear relationship between the state variables and the thermodynamic driving forces. Although linearity can only be guaranteed close to equilibrium, linear laws have historically worked well and so this assumption is assumed to be valid for all times [15]. The elements $M_{qq}$ and $M_{oo}$ are related to the thermal conductivity, $k=M_{qq}/T^2$, and the self diffusion coefficient of the interstitial oxygen, $D=M_{oo}k_b/C_o$ where $k_b$ is the Boltzmann's constant and $C_o$ is the concentration of interstitial oxygen atoms. Defining the flux in this way reconciles this development with the expression used by Lay [18] and the diffusion driving force of Darken [19]. The 'cross-terms' $M_{qo}$ and $M_{oq}$ are related to the Soret (thermodiffusion) and Dufour effects. In accordance with the Onsager reciprocal relationship, $M_{qo}$ and $M_{oq}$ are equal in magnitude. In this particular application, there are large temperature gradients present but not comparably large concentration gradients. Therefore, as a simplification, the Dufour term can be neglected. This system may be simplified through the heat of transport, $Q^*$ defined as [20]:

$$M_{oq}=M_{oo}Q^*, \tag{3}$$

which simplifies the flux expressions to the more traditional form:

$$\vec{q}=-k\vec{\nabla}T, \tag{4}$$

$$\vec{J}_o=-\frac{DC_o}{k_bT}\left(\nabla\mu_T+\frac{Q^*}{T}\nabla T\right). \tag{5}$$

### 2.2. Stefan formulation

The Stefan formulation is based on conservation of heat and mass flux across a moving phase change front. In the implementation for this work, the moving domain is transformed onto a stationary domain for computation via the Arbitrary Lagrange Eulerian method [21].

Fig. 2 shows the basic schematic of a two phase Stefan problem, defining the normal direction $\hat{n}$ and the rate of melting $R_{fus}$ in accordance with the convention in [22]. Solid and liquid properties are denoted by subscripts $S$ and $L$, respectively. The temperature profile in the sample is continuous across the boundary; however, a discontinuity in the heat flux, corresponding to absorption of latent heat, is present in the case of movement of the phase boundary. The oxygen profile is discontinuous at the boundary if the sample is hyperstoichiometric, the equilibrium concentrations in coexisting phases being given by the solidus and liquidus compositions at the local temperature.

The molar concentration of $UO_2$ is represented by $C$, assumed in the dilute limit to remain constant regardless of the interstitial oxygen mole fraction. Therefore, the mole fraction of interstitial oxygen to $UO_2$ is given by $x = C_o/C$.

Heat and mass balance must be satisfied in both the liquid and solid phases independently. Using the fluxes defined in Eqs. (4) and (5), this implies for both phases:

$$\rho C_P\frac{\partial T}{\partial t}=\vec{\nabla}\cdot(k\nabla T), \tag{6}$$

$$\frac{\partial C_o}{\partial t}=\vec{\nabla}\cdot\frac{DC_o}{k_bT}\left(\nabla\mu_T+\frac{Q^*}{T}\nabla T\right), \tag{7}$$

where $\rho$ is the density and $C_p$ is the heat capacity at constant pressure.

The gradient of the chemical potential (at constant temperature) may be expanded and converted into the expression used by Sari and Schumacher [23]:

$$\begin{aligned}C\tfrac{\partial x}{\partial t}&=\vec{\nabla}\cdot\tfrac{DC_o}{kT}\tfrac{\partial\mu}{\partial x}(\nabla x+\tfrac{Q^*}{\partial\mu/\partial x\cdot T}\nabla T)\\&=C\vec{\nabla}\cdot\tilde{D}(\nabla x+\tfrac{x}{1+(\partial\ln\gamma/\partial\ln x)}\tfrac{Q^*}{RT^2}\nabla T),\end{aligned} \tag{8}$$

where $\tilde{D}$ is the chemical diffusion coefficient of interstitial oxygen, $\gamma$ is the activity coefficient, and $R$ is the ideal gas constant.

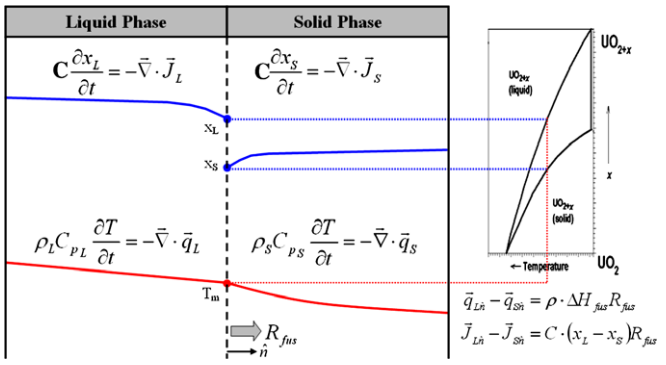


**Fig. 2.** Schematic diagram of the Stefan formulation applied to a coexisting solid and liquid phase, with a phase boundary indicated by the separating line.

The rate of fusion, corresponding to the rate of movement of the interface in Fig. 2, may be determined by a mass/energy balance across this interface. Using normal fluxes indicated by a subscript $\hat{n}$, the balanced equations may be written:

$$\vec{q}_{L\hat{n}} - \vec{q}_{S\hat{n}} = \rho \Delta H_{fus} R_{fus}, \tag{9}$$

$$\vec{J}_{L\hat{n}} - \vec{J}_{S\hat{n}} = C(x_L - x_S) R_{fus}, \tag{10}$$

where $H_{fus}$ is the enthalpy of fusion, $R_{fus}$ is the rate of fusion (melting), and $x_L$ and $x_S$ are the liquidus and solidus compositions.

### 2.3. Phase Field model

The Phase Field model introduces a variable $\varphi$ into the expressions for the thermodynamic functions to represent the local phase. It is converted to a volume fraction through a function $p(\varphi)$. As $\varphi$ varies continuously between 0 (solid) and 1 (liquid), a two phase 'mushy zone' is encountered in contrast to the sharp interface used in the Stefan formulation described above. Material properties between phases are expressed as a linear function of progression of $p(\varphi)$. The demarcation between solid and liquid may be deduced from the solution as the contour of $\varphi = 0.5$.

As derived in Appendix A, the Phase Field model requires the solution of the following set of partial differential equations:

$$\rho C_P \frac{\partial T}{\partial t} = -\vec{\nabla} \cdot \vec{q} - \frac{\partial h}{\partial \varphi} \frac{\partial \varphi}{\partial t}, \tag{11}$$

where $h$ is the enthalpy density.

The flux of oxygen is derived in a similar manner to Eq. (8) except, since the chemical potential is also a function of $\varphi$, the flux is derived including a term dependent on the gradient in $\varphi$. This term acts to maintain the solubility gap across the interface, and vanishes when the chemical potential is equal in both phases in accordance with phase equilibrium theory.

$$C \frac{\partial x}{\partial t} = C \vec{\nabla} \cdot \tilde{D} \left[ \nabla x + \frac{1}{\partial \mu / \partial x} \frac{Q^*}{T} \nabla T + \frac{\partial \mu / \partial \varphi}{\partial \mu / \partial x} \nabla \varphi \right]. \tag{12}$$

Finally, as shown in Appendix A, the following differential equation must be solved in order to determine the rate of phase change:

$$\frac{\partial \varphi}{\partial t} = -\frac{M_\varphi}{T} \left[ \frac{\partial g}{\partial \varphi} - \mu \frac{\partial x}{\partial \varphi} - T \varepsilon_\varphi^2 \vec{\nabla}^2 \varphi \right] + \dot{\varphi}_n, \tag{13}$$

where $\dot{\varphi}_n$ is the rate of nucleation, $M_\varphi$ is the mobility of $\varphi$, $\varepsilon_\varphi$ is a parameter which controls the width of the interface, and $g$ is the Gibbs energy density.

These equations can be seen to differ from those of the Stefan formulation by the addition of the variable $\varphi$, its rate of change and gradient, which account for the phase, latent heat liberation and the solubility gap between phases. The Stefan model accounts for these effects via the movement of the phase boundary. From inspection of Eq. (13), it can be seen that the rate of change of $\varphi$, is governed by a free energy minimization. In fact all three of the presented equations are derived from the principle of entropy maximization. A detailed explanation and derivation of $\dot{\varphi}_n$, $M_\varphi$, $\varepsilon_\varphi$ and other phase field parameters are given in [12].

## 3. Laser flash experiments

The current model is being validated against laser flash experiments conducted at the Institute for Transuranium Elements [9,24]. These experiments are designed to measure the melting transition in $UO_{2+x}$, but also include data that are useful for the current model validation. In these experiments, a prepared sample of $UO_{2+x}$ is held in a high pressure helium buffer gas in order to suppress vaporization of the sample. The sample is heated on one side with a high intensity laser beam until melting occurs. The intensity of the beam is then reduced to a lower level which prevents undercooling effects. The surface temperature of the sample is recorded as a function of time by optical pyrometry and is the main resulting data collected from the experiment.

The laser is assumed to deposit energy uniformly (within the laser spot) in accordance with the expression:

$$q_{laser} = \varepsilon \cdot P_{max} P_{pulse}(t), \tag{14}$$

where $P_{pulse}(t)$ is the laser power profile, $P_{max}$ is the maximum power of the laser beam and $\varepsilon$ is the emissivity which, through Kirchhoff's radiation law [25], is assumed to be equal to the absorbtivity.

Heat is lost from the surface of the sample with heat transfer through the buffer gas, radiative heat transfer and vaporization. Heat transfer in the buffer gas is modeled simultaneously to account for heat lost from the sample. The other terms are accounted for by the equation:

$$q_{loss} = \varepsilon \sigma_{SB} (T^4 - T_\infty^4) + H_{vap} \cdot J_{eff}, \tag{15}$$

where $T_\infty$ is the ambient temperature, $\sigma_{SB}$ is the Stefan Boltzmann's constant, $H_{vap}$ is the molar enthalpy of vaporization. The term $J_{eff}$ is the rate of molecular vapourization assumed to be small enough so as not to constitute a mass loss, but rather only a loss of heat.

$$J_{eff} = C_{eff} \left( \frac{44.3}{\sqrt{M}} \cdot \frac{P_{vap}}{\sqrt{T}} \right), \tag{16}$$

where $P_{vap}(T)$ is the vapour pressure [26] and $M$ is the molar mass of the vapour species. Eq. (15) is the Knudsen effusion formula [27] which is designed for effusion into a vacuum and is used as a simplification of the vapourization process. To correct this for the presence of the buffer gas, this formula includes a constant fraction $C_{eff}$ selected to reproduce the observed temperature profile.

## 4. Material properties

The Fink review [28] is taken as the primary source of the material properties, some of which must be extrapolated well beyond their quoted temperature range. Extrapolation of solid properties to the melting temperature is further complicated by the presence of the λ-transition at approximately 2670 K which may also affect the temperature dependence of the material properties. Of specific concern is the chemical diffusion coefficient of interstitial oxygen near the melting temperature in the solid and liquid phases.

The expression for the chemical diffusion coefficient in the solid is given as [13,29]:

$$\tilde{D} = 2.5 \cdot \exp(-16\ 400/T)\ \mathrm{cm^2/s}, \tag{17}$$

which is calculated from the oxygen self-diffusion coefficient of interstitial oxygen through application of the thermodynamic factor described earlier. This expression is presented as invariant with the oxygen concentration by virtue of the fact that the thermodynamic factor varies as $1/x$ whereas the self-diffusion coefficient varies approximately with $x$. The presence of the λ-transition and associated effects may affect this value at temperatures about 2670 K with molecular dynamics simulations [30] predicting an increase in the self-diffusion coefficient.

The liquid diffusion coefficient is also not well known, requiring the use of the Stokes–Einstein theory with oxygen atom diffusing through a viscous solvent of $UO_2$. Unfortunately, using the viscosity recommended by Fink, this yields a diffusion coefficient for oxygen in the liquid urania that is lower than that of the solid. As this is not typical, a more reasonable estimate is to use the value of the diffusion coefficient in the solid at the melting temperature.

## 5. Results

At present, the hyperstoichiometric model has only been solved for small deviations from stoichiometry in one dimension, considering the depth into the sample in the middle of the laser beam/molten pool. Radial symmetry about this axis is supported by the fact that the simulated depth of the molten pool is small compared to the radius of the laser beam. Radial effects have also been shown to be negligible in simulations of the stoichiometric case [12].

Figs. 3 and 4 assume that the diffusion coefficient in the solid is valid through the λ-transition up to the melting point. The liquid diffusion coefficient is assumed to be the same as that of the solid at the melting point.

It can be seen that there is a high level of agreement between the Stefan and Phase Field model both in terms of the surface temperature and stoichiometry profile. Both simulations reproduce the observed experimental results well but depart slightly from the observations at the end of the solidification region.

The simulation was repeated where the value of the solid (and therefore liquid) diffusion coefficient was held at 2670 K, the highest temperature to which Eq. (17) can reasonably be extrapolated. This simulation therefore provides the smallest diffusion coefficient that would be expected for both the liquid and solid phase. The resulting profile of surface oxygen vs. time was altered slightly, as would be expected, but the change on the temperature profile was negligible thereby indicating a small sensitivity to the diffusion coefficient on the model.

The sensitivity of the simulation to the thermal conductivity and density is thought to be the same as for the stoichiometric case investigated in [12]. In this case, the model is shown to be slightly sensitive to the thermal conductivity in the liquid, which has large uncertainty quoted in the literature. The model is further shown to be insensitive to changes in the chosen density.

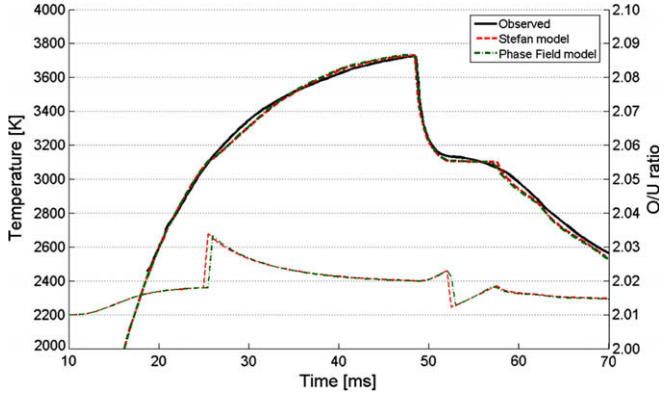


**Fig. 3.** Surface temperature and oxygen concentration results for $UO_{2.01}$.

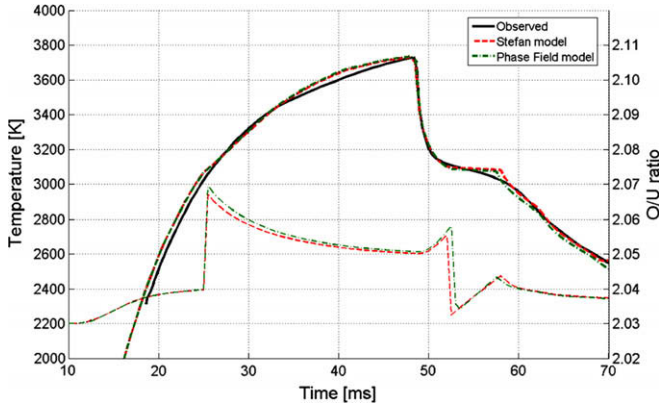


**Fig. 4.** Surface temperature and oxygen concentration results for $UO_{2.03}$.

## 6. Discussion

The close correspondence between model predictions indicate that the both the Stefan and Phase Field models are sound. The models predict the observed temperature well, although improvements are possible to better reproduce the complex solidification process. It can be noted that apart from the solidification region, the thermogram is well reproduced, indicating a good choice of boundary conditions.

Computationally, the Stefan model is less memory intensive and computes faster due to the implementation on the moving mesh. The Phase Field model requires a high degree of resolution over the entire domain of interest in order to adequately resolve the thin interface which significantly increases the computational requirements for the solution of the model. The Phase Field model can however be easily generalized to the two dimensional case due to its robust treatment for the interface geometries. The Stefan formulation suffers in this regard as the creation of an interface (as opposed to the movement of an interface described herein) poses a challenge that is further compounded by two dimensional effects.

Investigation of the sensitivity of the model to the diffusion coefficient shows a lack of sensitivity in the liquid region. This can be interpreted as implying that the diffusion coefficient in the liquid is very fast compared to the size of the liquid region, and so is capable of maintaining essentially steady state diffusion even at the lowest justified value. The sensitivity to the diffusion coefficient in the solid is slightly larger as it applies to a larger domain. The main factors affecting oxygen transport is therefore solute redistribution as a result of the phase change. This depends on the chosen phase diagram, which was not varied in the current analysis.

Although a slight modification of the phase diagram to better reproduce the experimental results can be considered, the change still does not fully reproduce all observations. As such, it is possible that radial effects must be considered in the simulation as the molten pool solidifies radially towards the centre of the pool as observed in the current experiments. These radial effects would enhance the solute redistribution and is the subject of further investigation. The assumptions in the derivation of the model may also lead to inaccurate prediction. Notably, the assumption of local equilibrium at the interface may not be completely correct if the solidification rate is sufficiently high and diffusion cannot reestablish the solubility gap between phases fast enough. This leads to the phenomenon of solute trapping, although this seems unlikely due to the high diffusion rates as previously discussed. The assumptions of a linear phenomenological law may also be questionable at such large temperature gradients and short times. Nonlinear laws are possible to implement, but are outside of the scope of the current work although the current treatment shows reasonable agreement with the experimental results.

## 7. Conclusions

The presented models show that both the Stefan and Phase Field models are mutually consistent and agree fairly well with the observations from laser flash experiments on slightly hyperstoichiometric $UO_{2+x}$. The models are derived from first principles in a method that is consistent with equilibrium thermodynamics, providing a strong connection between the evolution of the state

variables and their equilibrium values. The sensitivity of the models to uncertainty in the material properties is judged to be small.

These sophisticated models may now be used in order to assess the effects of simplifications particularly used in other codes to simulate molten fuel behaviour during severe fuel damage conditions where typically just the heat capacity is modified to represent the effect of molten material on the temperature predictions. The Phase Field model in particular lends itself well to the simulation of centreline melting of operational nuclear fuel, which is a focus of further development

## Acknowledgments

This work was funded by a Defence Research and Development Board [DRDB] scholarship and a Collaborative Research and Development grant from the Natural Sciences and Engineering Research Council of Canada [NSERC].

Laser flash experiments were carried out at JRC-ITU Karlsruhe within the 6th Framework Programme of the European Commission as a part of the action 'Safety of Nuclear Fuel'.

## Appendix A. The Theory of Irreversible Processes

The theory of irreversible processes is based on the conservation of internal energy and mass, and the requirement of positive entropy production for a real system that is not in equilibrium.

Assuming local equilibrium to exist in the case of a two-phase region, the local state can be written as a function of the internal energy $u$, the overall composition of interstitial oxygen $x$ and the phase $\varphi$. The liquidus and solidus compositions are determined by the relations $(1-p(\phi))x_s + p(\phi)x_L = x$ and $x_s = x_L k_p$ where $k_p$ is the partition coefficient. It is then possible to show that for a certain choice of the entropy functional, the rate of entropy production is given by the expression [31]:

$$s_{\text{prod}} = \vec{\nabla}\frac{\partial s}{\partial u}\cdot\vec{J}_u + \vec{\nabla}\frac{\partial s}{\partial x}\cdot\frac{\vec{J}_o}{C} + \left[\frac{\partial s}{\partial \varphi} + \varepsilon_\varphi^2\vec{\nabla}^2\varphi\right]\frac{\partial \varphi}{\partial t}, \tag{18}$$

where $s = s(u,x,\phi)$ is the entropy density expressed as a function of the internal energy $u = u(T,x,\phi)$, $x$ and $\varphi$. The internal energy flux is represented by $\vec{J}_u$ and the molar flux of interstitial oxygen by $\vec{J}_o$. The constant $\varepsilon_\varphi$ is strictly related to the interface tension and provides an energy penalty for regions of sharply changing $\varphi$ and so helps control the width of the interface.

In the current implementation, volumetric expansion is neglected and so the density is assume to be constant for all temperatures and phases. Neglecting nuclear reactions, the laws of conservation of energy and mass are:

$$\partial u/\partial t = -\vec{\nabla}\cdot\vec{J}_u, \tag{19}$$

$$\partial C_o/\partial t = -\vec{\nabla}\cdot\vec{J}_o, \tag{20}$$

where $C_o$ is the concentration of interstitial oxygen atoms.

The derivatives of entropy with respect to the state variables may be derived as:

$$\frac{\partial s}{\partial u} = \frac{1}{T}, \tag{21}$$

$$\frac{\partial s}{\partial x} = -\frac{1}{T}\frac{\partial g(T,x,\varphi)}{\partial x} = -\frac{1}{T}C\mu(T,x,\varphi), \tag{22}$$

$$\frac{\partial s}{\partial \varphi} = -\frac{1}{T}\left[\frac{\partial g(T,x,\varphi)}{\partial \varphi} - C\mu\frac{\partial x}{\partial \varphi}\right], \tag{23}$$

where $\mu$ is the chemical potential of interstitial oxygen.

Entropy production, as given in Eq. (18), can be divided via Currie's law into inequalities for the vector components (fluxes) and the evolution of the scalar phase field. Separately, they must both be non-negative:

$$\vec{\nabla}\frac{1}{T}\cdot\vec{J}_u - \vec{\nabla}\frac{\mu}{T}\cdot\vec{J}_o \geqslant 0, \tag{24}$$

$$-\frac{1}{T}\left[\frac{\partial g(T,x,\varphi)}{\partial \varphi} - C\mu\frac{\partial x}{\partial \varphi} - T\varepsilon_\varphi^2\vec{\nabla}^2\varphi\right]\cdot\frac{\partial \varphi}{\partial t} \geqslant 0. \tag{25}$$

Through the use of the thermodynamic relation:

$$\frac{\partial(\mu/T)}{\partial(1/T)} = \frac{\partial h}{\partial C_o}, \tag{26}$$

where $h$ is the enthalpy density, and recognizing the internal energy flux to be the sum of conductive heat flux and the heat flux resulting from solute movement: $\vec{q} = \vec{J}_u - \partial h/\partial C_o\cdot\vec{J}_o$, Eq. (24) can be rewritten in its simplest form:

$$-\frac{\vec{\nabla}T}{T^2}\cdot\vec{q} - \frac{\vec{\nabla}\mu_T}{T}\cdot\vec{J}_o \geqslant 0, \tag{27}$$

where $\vec{\nabla}\mu_T$ indicates that the differential is to be taken at constant $T$. Eq. (24) yields an expression for the rate of change of $\varphi$:

$$\dot{\varphi} = -\frac{M_\varphi}{T}\left[\frac{\partial g(T,x,\varphi)}{\partial \varphi} - C\mu\frac{\partial x}{\partial \varphi} - T\varepsilon_\varphi^2\vec{\nabla}^2\varphi\right]. \tag{28}$$

In order to recover the classical heat transport equation, Eq. (19) can be written:

$$\begin{aligned} \tfrac{\partial h}{\partial t} &\simeq \tfrac{\partial u}{\partial t} = -\vec{\nabla}\cdot\vec{J}_u, \\ \rho Cp\dot{T} + \tfrac{\partial h}{\partial x}\dot{x} + \tfrac{\partial h}{\partial \varphi}\dot{\varphi} &= -\vec{\nabla}\cdot\vec{q} - \vec{\nabla}\cdot\tfrac{\partial h}{\partial C_o}\vec{J}_o, \\ \rho Cp\dot{T} &= -\vec{\nabla}\cdot\vec{q} - \tfrac{\partial h}{\partial \varphi}\dot{\varphi}, \end{aligned} \tag{29}$$

where the definition $\partial h/\partial T = \rho Cp$ has been used and the gradient of the molar enthalpy is assumed to be negligible due to small concentrations.

## References

[1] C.M. Allison, G.A. Berna, L.J. Siefken, Draft preliminary report for comment: SCDAP/MOD1 theory and models, Idaho National Engineering Laboratory informal report, 1985.
[2] W.J. Camp, M.F. Young, J.L. Tomkins, J.E. Kelly, P.J. Maudlin, R.J. Henninger, MELPROG-PWR/MODO: A Mechanistic Code for Analysis of Reactor Core Melt Progression and Vessel Attack Under Severe Accident Conditions, NUREG/CR-4909 SAND85-0237 R3, Sandia National Laboratories, April 1987.
[3] H.E. Sills, ELOCA Fuel Element Behaviour During High-Temperature Transients, Atomic Energy of Canada Limited Report, AECL-6357, March 1979.
[4] M.S. Veshchunov, R. Dubourg, V.D. Ozrin, V.E. Shestak, V.I. Tarasov, R. Dubourg, G. Nicaise, Nucl. Eng. Des. 236 (2006) 179.
[5] M.S. Veshchunov, V.D. Ozrin, V.E. Shestak, V.I. Tarasov, J. Nucl. Mater. 362 (2007) 327.
[6] J.D. Higgs, B.J. Lewis, W.T. Thompson, Z. He, J. Nucl. Mater. 366 (2007) 99.
[7] B.J. Lewis, W.T. Thompson, F. Akbari, D.M. Thompson, C. Thurgood, J. Higgs, J. Nucl. Mater. 328 (2004) 180.
[8] J.C. Ramirez, M. Stan, P. Cristea, J. Nucl. Mater. 359 (2006) 174.
[9] D. Manara, C. Ronchi, M. Sheindlin, M. Lewis, M. Brykin, J. Nucl. Mater. 342 (2005) 148.
[10] R.E. Latta, R.E. Fryxell, J. Nucl. Mater. 35 (1970) 195.
[11] V. Atrazhev, M. Brykin, Study Contract No. 17644-2001-03F1SC KAR RU Final Report (ITU), 2001.
[12] M.J. Welland, B.J. Lewis, W.T. Thompson, J. Nucl. Mater. 376 (2008) 229.
[13] H. Matzke, J. Chem. Soc. Faraday Trans. 2 (83) (1987) 1121.
[14] M. Baichi, C. Chatillon, G. Ducros, K. Froment, J. Nucl. Mater. 349 (2006) 57.
[15] S.R. de Groot, P. Mazur, Non-Equilibrium Thermodynamics, Dover Publications, Inc., New York, 1984.
[16] Ch. Soret, Arch. Sci. Phys. Nat. 2 (1879) 48.
[17] L. Dufour, Arch. Sci. Phys. Nat. 45 (1872) 9.
[18] K.W. Lay, J. Am. Ceram. Soc. 53 (1970) 369.
[19] L.S. Darken, Diffusion, Mobility and Their Interrelation Through Free Energy in Binary Metallic Systems, AIME, 1948.
[20] M. Bober, G. Schumacher, Material transport in the temperature gradient of fast reactor fuels, in: E.J. Henley, J. Lewins (Eds.), Advances in Nuclear Science and Technology, Academic press, New York, 1973.
[21] J. Donea, H. Antonio, J.-Ph. Ponthot, A. Rodríguez-Ferran, The Encyclopedia of Computational Mechanics 413, Wiley, 2004.

[22] S. Kou, Transport Phenomena and Materials Processing, John Wiley, New York, 1996.
[23] C. Sari, G. Shumacher, J. Nucl. Mater. 61 (1976) 192.
[24] D. Manara, PhD thesis, University of Warwick, 2004.
[25] J.R. Welty, C.E. Wicks, R.E. Wilson, Fundamentals of Momentum Heat and Mass Transfer, third Ed., John Wiley, New York, 1984.
[26] M. Tetenbaum, P.D. Hunt, J. Nucl. Mater. 34 (1970) 86.
[27] B.J. Lewis, B.J. Corse, W.T. Thompson, M.H. Kaye, F.C. Iglesias, P. Elder, R. Dickson, Z. Liu, J. Nucl. Mater. 252 (1998) 235.
[28] J.K. Fink, J. Nucl. Mater. 279 (2000) 1.
[29] J.A. Meachen, Nucl. Energy 28 (1989) 221.
[30] E. Yakub, C. Ronchi, D. Staicu, J. Chem. Phys. 127 (2007).
[31] Z. Bi, R.F. Sekerka, Physica A 261 (1998) 95.